The Design of Hard Drive Slider Bearings

Problem presented by
Ferdinand Hendriks
IBM Research Division

Participants: Jon Chapman, Alistair Fitt, John King, Colin Please, Donald French, Scott Rimbey, Thomas Witelski, Susan Triantafillou, Warren Weckesser

Summary report prepared by Thomas Witelski

1. Introduction

We discuss the use of mathematical techniques for the study of viscous lubrication flow to improve the design of a critical component in computer disk drives. Magnetic data in a hard disk drive is stored and/or retrieved when an electronic read/write element passes over the surface of a rapidly rotating disk. It is important to minimize the contact between the read/write head and the moving disk surface, since such collisions can cause significant damage to both components. However, it is also desirable to minimize the separation between the head and the disk surface; this is called the flying height. Reducing the flying height allows for more precise positioning of the data, thereby increasing the disk storage capacity.

The electronic read/write head is mounted in a rigid air bearing slider block. Air passing through the gap between the slider and the disk creates a lifting force and allows the slider to fly at a desired height above the disk. To calculate the lift and flying height for most slider designs generally requires numerical solution [1, 3] of a partial differential equation. Our study focuses on a class of designs that can be examined using asymptotic analysis.

The new "Tango" design [5, 6] is a simple, easy-to-fabricate slider surface that yields an analytic asymptotic solution for the lifting force. This basic solution make the analysis of various effects on this class of sliders into a tractable problem. Following a derivation of the governing fluid dynamics equations, we consider the conditions needed on the Tango design parameters in order to achieve quasi-static equilibrium in level flight. Further, using boundary layer analysis, it is shown that appropriately designed inlet tapers can reduce variations in flying height due to variations in altitude and ambient pressure. Similarly, changes in the flying height due to relative disk-slider orientation changes can be minimized through the design of "skew insensitive" lifting surfaces.

2. Governing equations

The position and motion of the slider is directly tied to the lifting force generated by air passing under its lower surface. Here, we briefly review the equations governing the air flow, which themselves couple back to the geometry of the slider. The conservation

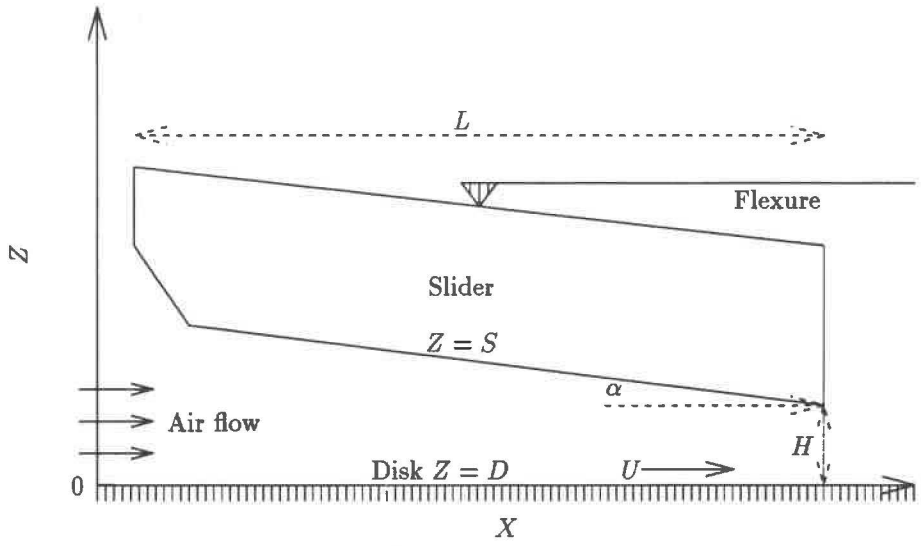

FIG. 1. *Geometry of the typical air bearing slider (side view).*

of momentum and mass for air in the gap between the slider and the disk surface are given by

$$\frac{D(\rho \mathbf{v})}{DT} = -\nabla P + \mu \nabla^2 \mathbf{v}, \qquad \frac{\partial \rho}{\partial T} + \nabla \cdot (\rho \mathbf{v}) = 0, \tag{2.1}$$

where ρ is the air density and $\mathbf{v}$ is the local velocity.

Of interest is the behavior of the air in the thin gap between the disk surface, $Z = D(X, Y, T)$, and the slider, $Z = S(X, Y, T)$ (see Figure 1). Generally, these surfaces are time-dependent to allow for dynamic effects. If the disk surface is not flat, then the distortions will propagate to the right with speed U. The slider is a rigid surface that is constrained by the flexure (the support arm); the slider position can be specified by giving the pitch angle α and the vertical displacement H (here indicated by the height of the read/write head). Outside the domain of the slider, the boundary condition on the flow is that the pressure returns to the uniform ambient level. The gap height under the slider has a very large aspect ratio; typical lengthscales are $L = 2 \times 10^{-3}$ m, with a comparable width of 1.5×10^{-3} m, and $\bar{H} = 50 \times 10^{-9}$ m, with a typical pitch angle of $\alpha = 300 \times 10^{-6}$ rad. Moreover, the disk surface and the air is moving with a large typical velocity $U = 10$ m/s. Consequently, lubrication theory can be applied to give a good approximation of the flow.

Following the lubrication approximation, and because the reduced Reynolds number $R_e(H/L)^2$ is very small, we can neglect inertial effects and assume that gradients in the vertical direction are much larger than gradients in the plane. The equation of conservation of momentum in the Z-direction shows that the pressure is independent of vertical position, $P = P(X, Y)$. Conservation of momentum in the X-Y plane yields the second order ordinary differential equation for the velocity,

$$\nabla P = \mu \frac{\partial^2 \mathbf{v}}{\partial Z^2}. \tag{2.2}$$

Applying no-slip boundary conditions at the disk surface and the slider surface,

$$\mathbf{v}(Z = D) = \mathbf{U}, \qquad \mathbf{v}(Z = S) = \mathbf{0} \tag{2.3}$$

yields the velocity field,

$$\mathbf{v} = \frac{\nabla P}{2\mu}(Z - D)(Z - S) + \mathbf{U}\left(1 - \frac{Z - D}{H}\right), \tag{2.4}$$

where the gap height H is defined by $H \equiv S - D$. Integrating the continuity equation in the vertical direction yields the overall mass balance,

$$\frac{\partial}{\partial T}(\rho H) + \nabla \cdot (\rho \mathbf{q}) = 0, \tag{2.5}$$

and the flux vector $\mathbf{q}$ is

$$\mathbf{q} = \int_D^S \mathbf{v}\, dZ = \frac{1}{2}H\mathbf{U} - \frac{1}{12\mu}H^3 \nabla P. \tag{2.6}$$

Combining these equations yields

$$\frac{\partial}{\partial T}(\rho H) + \tfrac{1}{2}\nabla \cdot (\rho H \mathbf{U}) = \frac{1}{12\mu}\nabla \cdot (\rho H^3 \nabla P). \tag{2.7}$$

Finally, for an isothermal ideal gas, density is proportional to pressure, so we may eliminate the density to yield the compressible Reynolds' equation,

$$\frac{\partial}{\partial T}(PH) + \tfrac{1}{2}\nabla \cdot (PH\mathbf{U}) = \frac{1}{12\mu}\nabla \cdot (PH^3 \nabla P). \tag{2.8}$$

We have neglected molecular slip conditions, which would modify the velocity boundary conditions, and introduce a (small) Knudsen number in the Reynolds equation.

Applying the scalings,

$$X = Lx, \qquad Y = Ly, \qquad Z = \bar{H}z, \qquad H = \bar{H}h,$$

$$P = P_A p, \qquad p_a = 1, \qquad T = Lt/U, \qquad \mathbf{U} = U\mathbf{u}$$

yields the nondimensionalized equation,

$$\frac{\partial}{\partial t}(ph) + \tfrac{1}{2}\nabla \cdot (ph\mathbf{u}) = \frac{1}{\Lambda}\nabla \cdot \left(ph^3 \nabla p\right) \tag{2.9}$$

where the bearing number is defined by

$$\Lambda = \frac{12\mu LU}{P_A \bar{H}^2}, \tag{2.10}$$

for our application $\Lambda \sim 20,000$. Consequently, we use ϵ, the inverse bearing number,

$$\epsilon = \frac{1}{\Lambda} \to 0, \tag{2.11}$$

as our small parameter for an asymptotic expansion of the solution in the limit of large disk velocity and small flying height.

The solid-body rotation of the hard drive platter yields a divergence-free velocity field, $\nabla \cdot \mathbf{u} = 0$, and further simplifies the Reynolds equation to

$$\frac{\partial}{\partial t}(ph) + \tfrac{1}{2}\mathbf{u} \cdot \nabla(ph) = \epsilon \nabla \cdot \left(ph^3 \nabla p\right). \tag{2.12}$$

Finally, using the phonetic substitution, $f = ph$,

$$f_t + \tfrac{1}{2}\mathbf{u} \cdot \nabla f = \epsilon \nabla \cdot \left(f\left(h\nabla f - f\nabla h\right)\right). \tag{2.13}$$

This is a singularly perturbed nonlinear advection-diffusion equation[1] that relates the slider shape h to the pressure through $p = f/h$. From the resulting pressure, we get the lifting force on the slider

$$\mathcal{L} = \int\int_{\Omega} (p(x,y) - p_a)\, dx\, dy, \tag{2.15}$$

and the pitching rotational moment,

$$\mathcal{M} = \int\int_{\Omega} (x - \bar{x})(p(x,y) - p_a)\, dx\, dy, \tag{2.16}$$

where Ω denotes the domain of the slider and $\bar{x}$ is the position of the axis of rotation imposed by the flexure (see Figure 1). The flexure is also responsible for applying a load force, w, on the slider to balance the lifting forces. These relations couple back into the mechanical force balances on the slider to determine the flying height and the slider orientation, $z = s(x,y,t)$.

We now obtain asymptotic solutions of (2.13) for a class of simple sliders. In particular, we examine the influence of boundary layer solutions on the ambient pressure sensitivity of the lifting force. Similarly, we will make use of the outer solution to determine the lifting force and pitching moment for Tango sliders in terms of their design parameters.

3. Asymptotics

Significant progress can be made in the study of one-dimensional or pseudo-one-dimensional slider surfaces without resorting to extensive numerical simulations. Equation (2.13) is an advection-diffusion equation; if the slider surface has rapid spatial variations in the cross-stream direction then diffusive boundary layers will result. These

[1] Note, that while the f form (2.13) of the Reynolds equation is strongly motivated by the form of the convective terms in (2.12), equation (2.13) isn't very well suited for numerical simulations of typical slider designs. Equation (2.13) contains second derivatives of h, which suggests that the numerics will have convergence and/or stability problems for typical slider designs with piecewise continuous h. For this application, a better form of the Reynolds equation is

$$\frac{\partial}{\partial t}(ph) + \tfrac{1}{2}\mathbf{u} \cdot \nabla(ph) = \tfrac{1}{2}\epsilon \nabla \cdot \left(h^3 \nabla(p^2)\right). \tag{2.14}$$

effects spread as they propagate in the downstream direction. If they spread to a significant extent and interact with other parts of the flow, the analysis of the problem becomes much more difficult. Unfortunately, many common slider designs include sharp "rails" running along the length of the slider and produce significant diffusive boundary layers [3]. For these designs, asymptotics is of limited help. However, for sliders that are uniform in the cross-stream y-direction or are smoothly varying in that direction, these diffusive boundary layers are not significant, and perturbation methods can be expected to yield accurate solutions.

In this section, we examine the steady-state solutions for one-dimensional sliders. The disk velocity is taken to be $\mathbf{u} = \mathbf{a_x}$. A uniform flat disk surface, $d = 0$ will be assumed. Consequently, the gap height and the slider surface are equivalent, $s(x) = h(x)$, for the domain of the slider, $0 < x < 1$. For this problem, equation (2.13) reduces to

$$\frac{df}{dx} = 2\epsilon \frac{d}{dx}\left(f\left(h\frac{df}{dx} - f\frac{dh}{dx}\right)\right). \tag{3.1}$$

We will initially assume that the slider is smooth $h'(x) = o(\epsilon^{-1})$, then we will also study the influence of induced boundary layers for non-smooth $h(x)$.

3.1. Outer solution

In the limit $\epsilon \to 0$, the leading order outer solution is $f_0 = C$, or

$$ph = C, \tag{3.2}$$

where C is some constant. At the next order, $O(\epsilon)$ corrections that are proportional to the gradients of the slider profile are added to the solution. The appropriate boundary condition for the Reynolds equation is to specify the pressure all along the boundary of the slider. The boundary pressure is the constant ambient air pressure p_a, where we have taken the ground-level standard atmospheric pressure to be $p_a = 1$. From (3.2) it is clear that unless the boundary heights of the slider, $h_0 = h(0)$ and $h_1 = h(1)$, are identical, the solution will have a boundary layer.

3.2. Trailing boundary layers

In order to determine the correct constant of integration for the outer solution (3.2), we must determine where possible boundary layers can occur. Rescaling variables by

$$\tilde{x} = \frac{x - x_*}{\epsilon}, \qquad \tilde{f}(\tilde{x}) = f(x), \tag{3.3}$$

and integrating (3.1) once yields the inner problem

$$\frac{d\tilde{f}}{d\tilde{x}} = \frac{1}{2h_*}\left(1 - \frac{f_0}{\tilde{f}}\right), \tag{3.4}$$

where $h_* = h(x_*)$, for smooth $h(x)$. This is a first order differential equation and can only have monotone increasing or decreasing solutions, hence no internal layers are

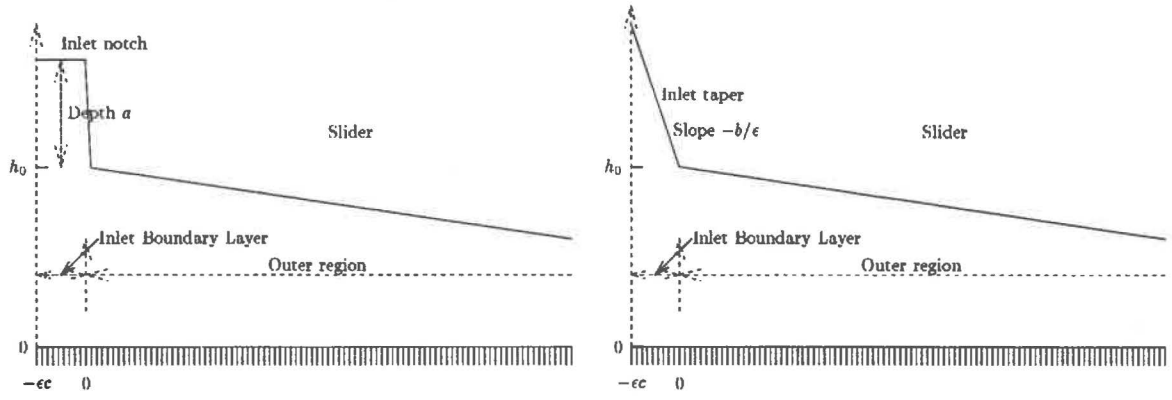

FIG. 2. *Schematic of notch and taper inlet boundary layer designs*

possible. From linear stability analysis at $\tilde{f} = f_0$, it is clear that for $f_0 > 0$ only a right boundary layer is possible; for $f_0 < 0$ only a left boundary layer is possible. The case of physical interest is $f_0 > 0$ ($ph > 0$), hence the outer solution is

$$f_0 = p_a h_0, \tag{3.5}$$

where $h_0 = h(0)$, the inlet height, and the trailing edge boundary layer solution in implicit form is

$$x(f) = 2\epsilon h_1 \left(f - f_1 + f_0 \ln \left| \frac{f - f_0}{f_1 - f_0} \right| \right) + 1, \tag{3.6}$$

where $f_1 = p_a h_1$. Interestingly, this result is independent of the relative values of h_0 and h_1, meaning that it is true for "converging" or "diverging nozzle" slider shapes, though the diverging shapes yield negative lifts and are not useful for this application. Neglecting the boundary layer contribution, the leading order lifting force is

$$\mathcal{L} = p_a \int_0^1 \left(\frac{h_0}{h(x)} - 1 \right) dx + O(\epsilon). \tag{3.7}$$

We will now examine the consequences of using a non-smooth slider surface.

3.3. Inlet boundary layers

Consider the influence of a non-smooth leading edge on an otherwise smooth slider shape. Consider adding two forms of inlet boundary layers in front of the smooth slider surface; first, a sharp, finite notch (see Figure 2a)

$$h(x) = \begin{cases} h_0 + a & -\epsilon c < x < 0 \\ h_0 - x & 0 < x < 1 \end{cases} \tag{3.8}$$

and second, a sharp taper (see Figure 2b)

$$h(x) = \begin{cases} h_0 - bx/\epsilon & -\epsilon c < x < 0 \\ h_0 - x & 0 < x < 1 \end{cases} \tag{3.9}$$

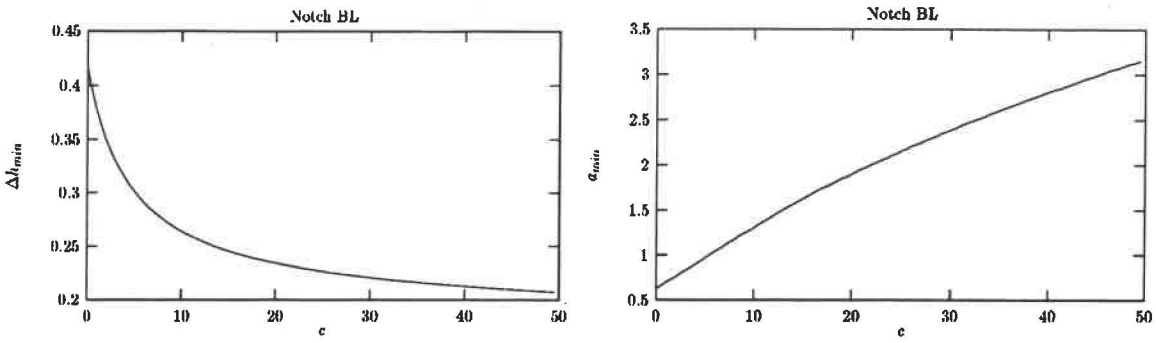

FIG. 3. *Decreased pressure sensitivity for the notch inlet boundary layer.*

these are sharp step or ramp distributions for $h(x)$. In these models, c is the width of the inlet layer and a, b give a measure of the jump in the surface due to the inlet. Rescaling for a boundary layer at $x = 0^-$, $\tilde{x} = x/\epsilon$, we obtain inner problems analogous to (3.4); for the notch,

$$\frac{d\tilde{f}}{d\tilde{x}} = \frac{1}{2(h_0 + a)}\left(1 - \frac{f_0}{\tilde{f}}\right), \tag{3.10}$$

and for the taper,

$$\frac{d\tilde{f}}{d\tilde{x}} = \frac{1}{2(h_0 - b\tilde{x})}\left(1 - \frac{f_0}{\tilde{f}} - 2b\tilde{f}\right). \tag{3.11}$$

As in the analysis of section 3.2, these inner problems yield right boundary layers that end at $x = 0$. However, here the effect of the boundary layer is significant because it will determine the value of f_0 for the outer solution, and thereby can significantly change the overall slider lift. In the following section we demonstrate the influence of induced leading edge boundary layer on the lift force as a function of the ambient pressure p_a.

Note that the pressure along the slider is a continuous function,but f can be discontinuous if h is discontinuous. This issue is significant for matching the boundary layers to the outer solution. For the taper, $h(x)$ is continuous, so the relation between the boundary layer at $\tilde{x} = 0^-$, $\tilde{f} = f_*$, and the outer solution is $f_* = f_0$. For the notch, the slider profile is discontinuous, yielding the matching condition

$$f_* = f_0\left(1 + \frac{a}{h_0}\right). \tag{3.12}$$

3.4. Decreased pressure sensitivity

To determine the effect of the boundary layer when the ambient pressure is varied, we consider the following comparison process. For a given boundary layer configuration, specified by the parameters (a, c) or (b, c), we select an appropriate applied load w to balance the lift (3.7) so that at standard atmospheric pressure, $p_a = 1$, the ideal flying height is achieved. This will make the trailing edge of the slider take the value 1 while the height at the front will have the value h_0. In practive h_0 has some $O(1)$ finite value.

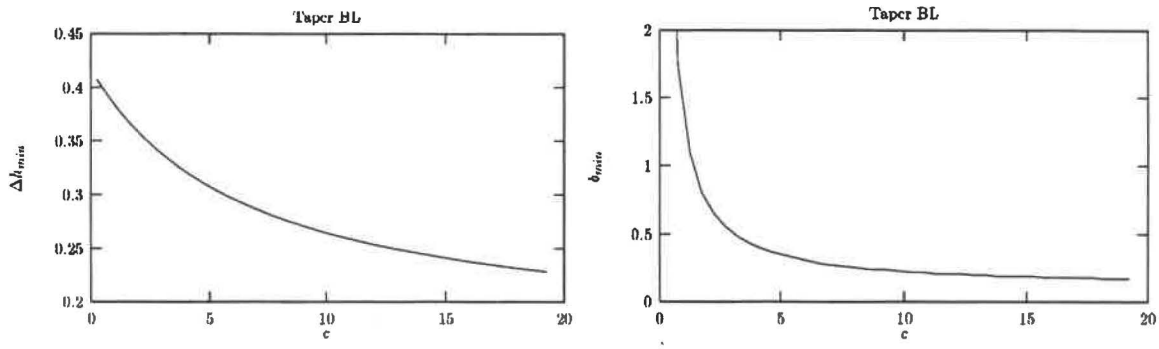

FIG. 4. *Decreased pressure sensitivity for the taper inlet boundary layer.*

To illustrate a possible method of decreasing the variation in the trailing edge flying height with the ambient pressure, we take $h_0 = 2$.

Integrating the inner problems across the boundary layer yields equations for the effective inlet pressure, for the notch

$$\tilde{f} + f_0 \ln|\tilde{f} - f_0|\Big|_{p_a(h_0+a)}^{f_0(1+a/h_0)} = \frac{c}{2(h_0+a)}, \tag{3.13}$$

and for the taper

$$\tfrac{1}{2}\ln|2b\tilde{f}^2 - \tilde{f} + f_0| + \frac{1}{\sqrt{8bf_0-1}}\arctan\left(\frac{4b\tilde{f}-1}{\sqrt{8bf_0-1}}\right)\Big|_{p_a(h_0+bc)}^{f_0} = \ln\left|\frac{h_0}{h_0+bc}\right|. \tag{3.14}$$

Solving each of these nonlinear equations yields a relation between the gap height for the outer solution h_0 and the effective inlet pressure f_0. These numerical calculations are summarized in Figures 3 and 4. Interest in this analysis stems from the fact that large variations in ambient pressure are commonly associated with operation at different altitudes. Hard drives in laptops used in airplanes typically experience a pressure that drops from $p_a = 1$ at ground level to $p_a = 2/3$ at cruising altitudes. This decreased pressure level yields lower lift forces, and smaller gap height and a greater possibility of disk head crash.

To assess the improvment due to the inlet boundary layer we consider the variation in flying height, Δh, defined as the difference between h_0 at $p_a = 1$ ($h_0 = 2$) and the h_0 subject to $p_a = 2/3$. If $c = 0$, then the design has no inlet boundary layer, and $\Delta h \sim 0.42$. By searching through the ranges of parameters (a, c) or (b, c) that define the inlets, we can find an optimal design a_{min} or b_{min} at each value of c that minimizes Δh to yield Δh_{min} The figures go on to show that by picking an optimal boundary layer design, we can reduce Δh to about 0.2 – approximately a 50% improvement!

4. Tango slider design

In this section we consider the one-dimensional "Tango" slider design. The Tango name originates from the fact that the slider has two distinct lifting surfaces that create balances in forces and torques. The two piecewise constant surfaces in the design are

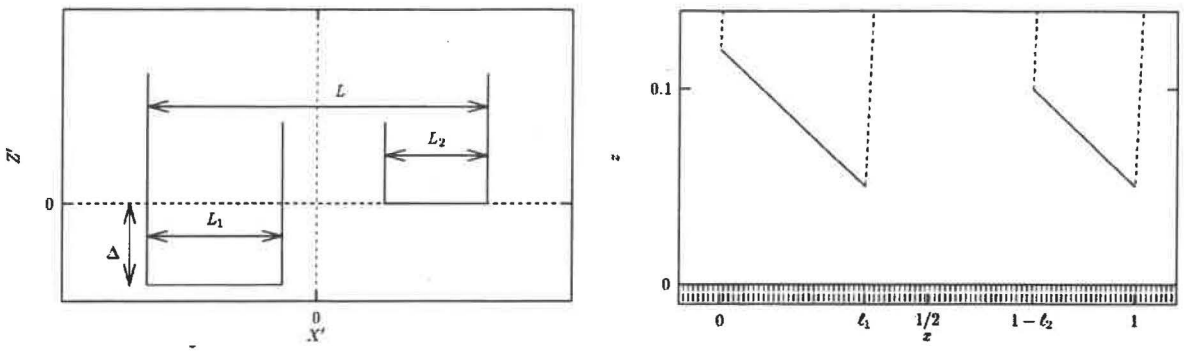

FIG. 5. *The Tango slider design: a) design parameters, b) the slider in level flight orientation.*

shown in Figure 5a, in dimensional units,

$$Z' = \begin{cases} -\Delta & -L/2 < X' < -L/2 + L_1, \\ 0 & L/2 - L_2 < X' < L/2. \end{cases} \tag{4.1}$$

In actual operation, the slider is elevated to some flying height H above the disk and is tilted with an angle of attack α. Following the appropriate translation and rotation, the slider profile can be nondimensionalized using the scalings

$$\Delta = \bar{H}\delta, \qquad L_1 = L\ell_1, \qquad L_2 = L\ell_2. \tag{4.2}$$

Further, in light of the large aspect ration, $\bar{H}/L$, and the small angle of attack, we rescale α, and finally obtain the profile (see Figure 5b),

$$\bar{\alpha} = \alpha L/\bar{H} \tag{4.3}$$

$$z = \begin{cases} \bar{h} - \bar{\alpha}x - \delta & 0 < x < \ell_1 \\ \bar{h} - \bar{\alpha}x & 1 - \ell_2 < x < 1 \end{cases} \tag{4.4}$$

To calculate the lifting force and pitching moment for this slider, we use the leading order outer solution derived earlier, $f_0 = ph_0$ to determine the pressure on each lifting surface. We assume that the pressure at the inlet of the second surface, $x = 1 - \ell_2$ is the same ambient level as at the inlet of the first surface, $x = 0$. Consequently, the force balance is

$$\int_0^{\ell_1} \left(\frac{\bar{h} - \delta}{\bar{h} - \delta - \bar{\alpha}x} - 1 \right) dx + \int_{1-\ell_2}^{1} \left(\frac{\bar{h} - \bar{\alpha}(1-\ell_2)}{\bar{h} - \bar{\alpha}x} - 1 \right) dx = w, \tag{4.5}$$

where w is the nondimensionalized applied load, and the moment balance is

$$\int_0^{\ell_1} (x - \bar{x}) \left(\frac{\bar{h} - \delta}{\bar{h} - \delta - \bar{\alpha}x} - 1 \right) dx + \int_{1-\ell_2}^{1} (x - \bar{x}) \left(\frac{\bar{h} - \bar{\alpha}(1-\ell_2)}{\bar{h} - \bar{\alpha}x} - 1 \right) dx = 0, \tag{4.6}$$

where $\bar{x} = 1/2$ is the flexure pivot position.

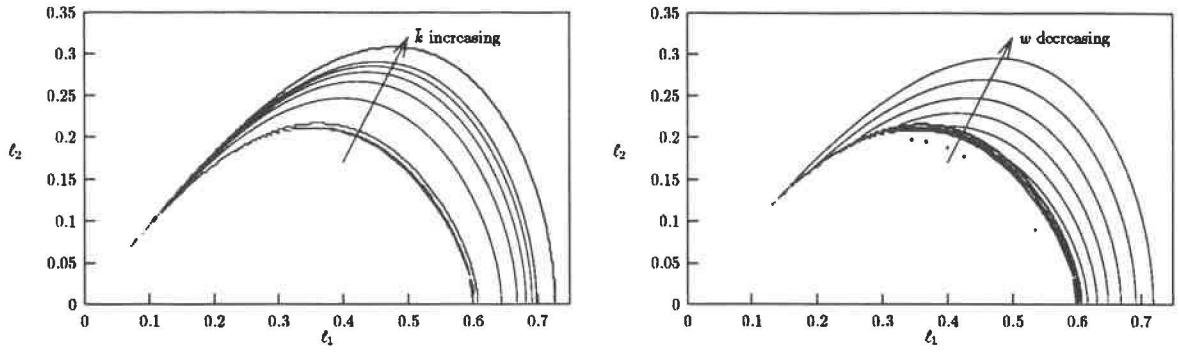

FIG. 6. *Equilibrium, level flight Tango design parameters: (a) Contour lines of the ratio* $\bar{k}(\ell_1, \ell_2) = \bar{h}/\bar{\alpha}$, *(b) Contours lines of the applied load* $w(\ell_1, \ell_2)$.

4.1. Equilibrium formulas

Analytic formulas for the equilibrium state of the slider would be very useful in the design process. By integrating the above force and moment balance equations, we obtained the following equations relating the design parameters $\bar{\alpha}$, $\bar{h}$, w, ℓ_1, and ℓ_2,

$$1 = \frac{\bar{h} - \delta - \bar{\alpha}\ell_1}{\bar{h}_1} \exp\left\{\frac{\bar{\alpha}}{\bar{h}_1}\left(\ell_1 + \frac{1}{2\delta}\left[(2\bar{h} - \bar{\alpha})w - \bar{\alpha}g\right]\right)\right\} \tag{4.7}$$

$$1 = \frac{\bar{h} - \bar{\alpha}}{\bar{h}_2} \exp\left\{\frac{\bar{\alpha}}{\bar{h}_2}\left(\ell_2 + \frac{1}{2\delta}\left[(2\bar{h} - \bar{\alpha} + 2\delta)w - \bar{\alpha}g\right]\right)\right\} \tag{4.8}$$

where $g(\ell_1, \ell_2) = \ell_1^2 + \ell_2^2$ and the inlet gap heights for the two surfaces are

$$\bar{h}_1 = \bar{h} - \delta, \qquad \bar{h}_2 = \bar{h} - \bar{\alpha}(1 - \ell_2). \tag{4.9}$$

Given, say, ℓ_1, ℓ_2, δ and w, the remaining parameters, α and $\bar{h}$, can be found using Newton's method. We also explored letting $\ell_1 = \ell + \epsilon$ and $\ell_2 = \ell$ where $\epsilon > 0$ in an attempt to solve the equations via a perturbation approach.

Often it is desired that the slider operate under "level flight" conditions, i.e. that the lowest points on the surface (in this case, the trailing edges of the two lifting surfaces) be at the same height above the disk surface. This condition yields the relation

$$\delta = \bar{\alpha}(1 - \ell_1). \tag{4.10}$$

It can be shown that (4.7,4.8) are degenerate for level flight solutions; if we write $\bar{h} = \bar{k}\bar{\alpha}$, then $\bar{\alpha}$ cancels out of both equations. What results is a system that yields $\bar{k}(\ell_1, \ell_2)$ for a level flight design and the corresponding unique value of the applied load $w(\ell_1, \ell_2)$ (see Figure 6). We observe that realistic physical solutions with $\bar{k} > 1/2$ only exist in a crescent-like area of the ℓ_1-ℓ_2 plane.

4.2. Quasi-Static Stability

If $m(\alpha) = m_1(\alpha) + m_2(\alpha)$ is the total moment we say the slider bearing is stable if $\partial m/\partial\alpha \leq 0$. Differentiating the integral formulas for the m_i's and manipulating the

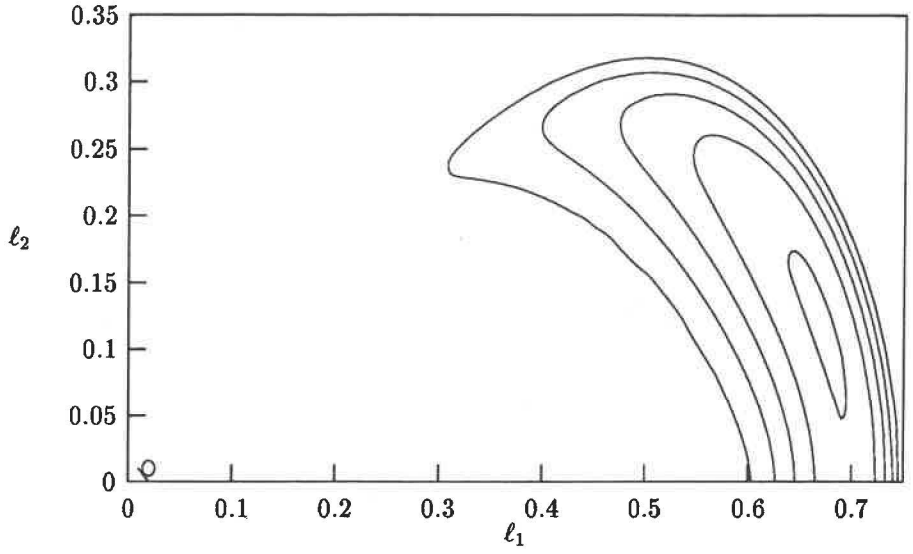

FIG. 7. *Contour lines of the pitching stiffness, $\partial m/\partial\alpha$, for level flight Tango slider at a fixed flying height. The stiffness increases towards the interior of the region.*

equation we can show that

$$\begin{aligned}\frac{\partial m}{\partial \alpha} \;\le\; & \ell_1\left(\frac{1}{4z_a}-\frac{1}{2\alpha}\right)+\frac{h-(1-\ell_1)\alpha}{2\alpha^2}\ln\frac{z_a}{z_a-\ell_1\alpha} \\ & +\; \ell_2(\tfrac{1}{2}-\ell_2)\left(\frac{\frac{1}{2}-\ell_2}{z_c}+\frac{1}{\alpha}\right)-\frac{(\frac{1}{2}-\ell_2)h}{\alpha^2}\ln\frac{z_c}{z_c-\ell_2\alpha}\end{aligned} \tag{4.11}$$

where

$$z_a = h-\frac{1}{2}\alpha+\ell_1\alpha, \qquad z_c = h-\frac{1}{2}\alpha+\ell_2\alpha.$$

This formula can be simplified by using the inequality

$$\ln(1-x)\le -x.$$

It then follows that $\partial m/\partial\alpha \le 0$ for $\ell_1 \le 1-h/\alpha$ and $\ell_2 \le 1/2$. Numerical calculation of the stiffness based on the exact equations is shown in Figure 7.

5. Skew insensitive designs

As the read/write head is moved from the inner track of the hard drive to the outer track, there is a change in orientation of the slider relative to the local disk velocity **u**. This is measured in terms of the skew angle which is the angle between the slider arm and **u** (see Figure 8). IBM seeks sliders that maintain a constant flying height and roll angle for all allowable skew angles. A high resistance to rolling at all skew angles and symmetry are also desirable slider properties. As a step toward these goals, we established a search procedure to find pad shapes, Ω, that minimize the variation in the lifting force over the range of allowable skew angles. We implemented this procedure for a special class of shapes and obtained the optimized pad shape presented here.

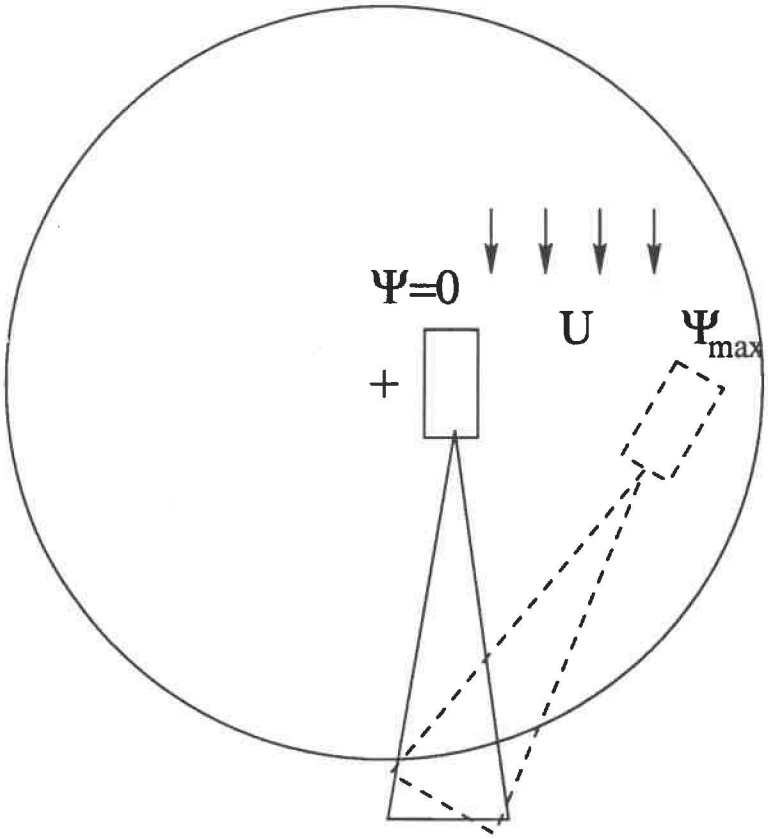

FIG. 8. *Top view of a hard disk drive, showing the range of skew angles, ψ as the slider is moved from the inner to outer tracks of the hard drive.*

For this calculation, the flying height is fixed and the roll angle is set to zero. The lift calculation is based on the two-dimensional steady, outer form of the Reynolds equation

$$\mathbf{u} \cdot \nabla f = 0, \tag{5.1}$$

which leads to the lift expression,

$$\mathcal{L}(\psi) = p_a \int\int_{\Omega} \left(\frac{h_i(\psi)}{h(x,y)} - 1 \right) dx\, dy, \tag{5.2}$$

where and $h_i(\psi)$ is the inlet (or leading edge) slider flying height, and in general can depend on the skew angle ψ. Our method for shape optimization minimizes the objective function

$$\mathcal{F}(\Omega) = \int_0^{\psi_{max}} \Big(\mathcal{L}_0 - \mathcal{L}(\Omega, \psi) \Big)^2 d\psi \tag{5.3}$$

subject to the constraint,

$$\mathcal{G}(\Omega) \equiv \mathcal{L}_0 - \mathcal{L}(\Omega, 0) = 0, \tag{5.4}$$

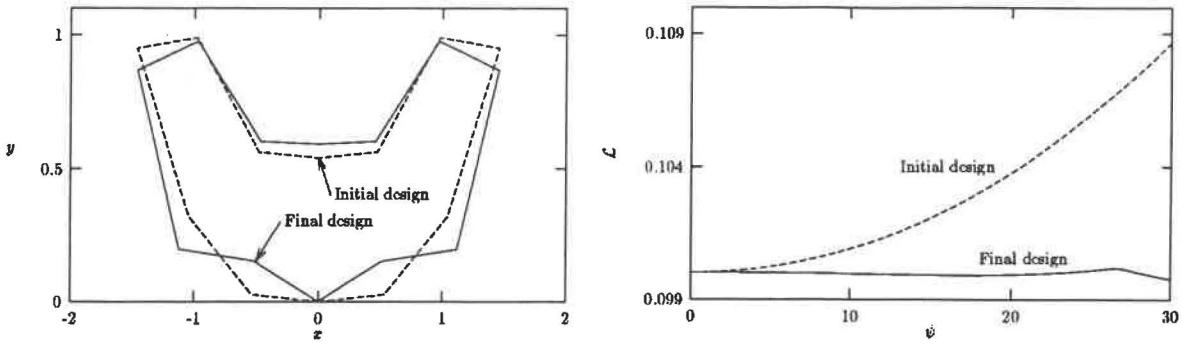

FIG. 9. *Skew insensitive designs: (a) initial and final pad designs, (b) corresponding variations in the lift as a function of the skew angle ψ (in degrees).*

where $\mathcal{L}_0$ is a constant. It should be noted that there are shapes known to give $\mathcal{F} = 0$.

The pad shape is restricted to a symmetric, polygonal pad centered on a slider. The pad design, $\mathbf{d}$, is defined as the set of x and y coordinates of the vertices. This specification admits known designs of constant lift. The optimization procedure iteratively improves $\mathcal{F}(\Omega) = F(\mathbf{d})$ by stepping through design space such that $\mathcal{G}(\Omega) = G(\mathbf{d}) = 0$ at each iteration. An initial design is found by adjusting a proposed design, $\mathbf{d}_0^0$, until it satisfies the constraint. Adjustments are made according to

$$\mathbf{d}_0^{(n+1)} = \left(\mathbf{d}_0^{(n)} - \frac{G}{|\nabla G|^2}\nabla G\right) \to \mathbf{d}_0, \qquad n = 0, 1, 2, \ldots \tag{5.5}$$

where

$$\nabla G = \left(\frac{\partial G}{\partial \mathrm{d}(1)}, \frac{\partial G}{\partial \mathrm{d}(2)}, \ldots\right), \tag{5.6}$$

where $\mathbf{d}(i)$ is the i-th component of the design vector. This is essentially Newton's scalar method applied in the direction $\nabla G/|\nabla G|$.

To improve a constraint-satisfying pad, a step in design space is taken in the direction,

$$-\nabla F_p = -\nabla F + \frac{\nabla F \cdot \nabla G}{|\nabla G|^2}\nabla G, \tag{5.7}$$

which is the result of projecting $-\nabla F$ onto the space normal to ∇G. A small step in this direction produces a design that decreases F while almost satisfying $G = 0$. The improved design is then adjusted by the procedure described above to meet the constraint. This iteration procedure is continued until F reaches a specified value or ∇F is approximately zero.

This procedure was applied to the initial design shown in Figure 9a. For this calculation the following parameters were used: $p_a = 10^5 \mathrm{N/m}^2$, $\mathcal{L}_0 = 0.1\mathrm{N}$, flying height = 50nm, and angle of attack = 300μrad. The variation of lift with skew angle for this design is shown in Figure 9b. The design produced by the optimizer and the corresponding lift variation are shown on the same figures.

The result shows that a pad can be deformed into a nearly constant lift pad that differs from the previously known constant lift pads. The method used here provides a starting point for a more realistic calculation that accounts for variations in fly height and roll angle. More realistic pad shapes can be achieved by simply increasing the number of sides in the polygonal pad, which amounts to adding design parameters.

REFERENCES

[1] D.-H. CHOI AND S.-J. YOON, *Static analysis of flying characteristics of the head slider by using an optimization technique*, Journal of Tribology, 116 (1994) 90–94.

[2] M. TOKUYAMA AND S. HIROSE, *Dynamic flying characteristics of magnetic head slider with dust*, Journal of Tribology, 116 (1994) 95–100.

[3] J. W. WHITE, *Flying characteristics of the zero-load slider bearing*, Journal of Lubrication Technology, 105 (1983) 484–490.

[4] J. CHANDRA AND P. W. DAVIS, "Applications of differential inequalities to gas lubrication theory," in *Nonlinear Phenomena in Mathematical Sciences*, V. Lakshmikantham editor, Academic Press, New York (1982).

[5] F. Hendriks, Speed-dependence, take-off, and stiction of a new class of gas bearing sliders, *Tribology Transactions* 39, 3 (1996) pp. 603–608.

[6] F. Hendriks, V.D. Khanna, R.M. Crone, U.S. Patent #5,424,888, Speed Independent, Air Bearing Slider.